Original Article

JCBFM

Journal of Cerebral Blood Flow & Metabolism
2020, Vol. 40(4) 799–807

DOI: 10.1177/0271678X19843776
journals.sagepub.com/home/jcbfm
SAGE

A PET study in healthy subjects of brain exposure of ^{11}C-labelled osimertinib – A drug intended for treatment of brain metastases in non-small cell lung cancer

Andrea Varrone[1], Katarina Varnäs[1], Aurelija Jucaite[1,2], Zsolt Cselényi[1,2], Peter Johnström[1,2], Magnus Schou[1,2], Ana Vazquez-Romero[1], Mohammad M Moein[1], Christer Halldin[1], Andrew P Brown[3], Karthick Vishwanathan[4] and Lars Farde[1,2]

Abstract

Osimertinib is a tyrosine kinase inhibitor (TKI) of the mutated epidermal growth factor receptor (EGFRm) with observed efficacy in patients with brain metastases. Brain exposure and drug distribution in tumor regions are important criteria for evaluation and confirmation of CNS efficacy. The aim of this PET study was therefore to determine brain distribution and exposure of ^{11}C-labelled osimertinib administered intravenously in subjects with an intact blood–brain barrier. Eight male healthy subjects (age 52 ± 8 years) underwent one PET measurement with ^{11}C-osimertinib. The pharmacokinetic parameters $C_{max\ (brain)}$ (standardized uptake value), $T_{max\ (brain)}$ and $AUC_{0–90\,min\ brain/blood\ ratio}$ were calculated. The outcome measure for ^{11}C-osimertinib brain exposure was the total distribution volume (V_T). ^{11}C-osimertinib distributed rapidly to the brain, with higher uptake in grey than in white matter. Mean C_{max}, T_{max} and $AUC_{0–90\,min\ brain/blood\ ratio}$ were 1.5 (range 1–1.8), 13 min (range 5–30 min), and 3.8 (range 3.3–4.1). Whole brain and white matter V_T were 14 mL × cm^{-3} (range 11–18) and 7 mL × cm^{-3} (range 5–12). This study in healthy volunteers shows that ^{11}C-osimertinib penetrates the intact blood–brain barrier. The approach used further illustrates the role of molecular imaging in facilitating the development of novel drugs for the treatment of malignancies affecting the brain.

Keywords

Brain metastasis, microdose, PET, epidermal growth factor receptor, blood–brain barrier

Received 9 January 2019; Revised 5 March 2019; Accepted 11 March 2019

Introduction

Lung cancer has long been the most common cause of death from cancer in the world. Of all lung cancers, non-small cell lung cancer (NSCLC) is the most common and represents 80% to 85% of all cases. At time of diagnosis, approximately 70% of patients with NSCLC already have locally advanced or metastatic disease not amenable to surgical resection.[1]

During the past decade, the understanding of the critical role of the epidermal growth factor receptor (EGFR) pathway and subsequent development of EGFR-targeted tyrosine kinase inhibitors (EGFR-TKI) have led to significant advancements in the

[1]Department of Clinical Neuroscience, Centre for Psychiatry Research, Karolinska Institutet and Stockholm County Council, Stockholm, Sweden
[2]PET Science Centre, Precision Medicine and Genomics, IMED Biotech Unit, AstraZeneca, Karolinska Institutet, Stockholm, Sweden
[3]Global Medicines Development Oncology, AstraZeneca, UK
[4]Quantitative Clinical Pharmacology, Early Clinical Development, IMED Biotech Unit, AstraZeneca, Waltham, MA, USA

Corresponding author:
Andrea Varrone, Department of Clinical Neuroscience, Centre for Psychiatry Research, Karolinska Institutet and Stockholm County Council, R5:02 Karolinska University Hospital, Stockholm SE-17176, Sweden.
Email: andrea.varrone@ki.se

treatment of NSCLC. EGFR-TKIs are now the established first line therapy in patients with NSCLC having sensitizing mutations in EGFR (EGFRm), the most common of which are L858R and deletions in exon 19 [Ex19del].[2,3] Selective inhibition of EGFR-TKI has demonstrated objective response in approximately 70% of patients with advanced NSCLC harboring the sensitivity mutations.

The two major problems in NSCLC are that albeit an initial response to first or second generation EGFR-TKIs, patients subsequently develop resistance to therapy, with a median time to progression of ~10 months.[4] In about 30–40% of cases, patients also develop brain metastases during treatment with EGFR-TKIs.[5–9] In approximately 50% of those initially responsive to first or second generation EGFR-TKI patients, disease progression is associated with the emergence of a secondary EGFR mutation, T790M in exon 20 of the EGFR that confers resistance to therapy.[10]

Osimertinib is a potent, oral and irreversible third-generation EGFR-TKI that has shown to provide clinical benefit to patients with advanced NSCLC harboring the single sensitivity mutations as well as the resistance mutation following prior therapy with first or second generation EGFR-TKIs.[11,12] Osimertinib has shown efficacy superior to that of first generation EGFR-TKIs (erlotinib and gefitinib) in the first-line treatment of EGFR mutation-positive advanced NSCLC (median PFS of 18.9 months compared to 10 months with erlotinib/gefitinib) and also a reduced risk of metastases.[4,13,14] Importantly, a number of clinical reports has described that osimertinib can provide rapid and sustained effect on brain metastases in individual cases[13,15–17] and reduced risk of CNS progression compared with standard EGFR-TKIs.[18] Thus, further understanding of the pharmacological properties of osimertinib that enable clinical efficacy for the treatment of CNS metastases is warranted.

In experimental animals, osimertinib has demonstrated higher brain exposure than gefitinib or erlotinib at clinically relevant doses and has, moreover, been found to induce sustained tumor regression in an EGFR mutation-positive PC9 (exon 19 deletion) mouse brain metastases model.[19] PET studies performed in non-human primates using ^{11}C-osimertinib (N-(2-((2-(dimethylamino)ethyl)(methyl)amino)-4-^{11}C-methoxy-5-(4-(1-methyl-1H-indol-3-yl)pyrimidin-2-ylamino)phenyl)acrylamide) have also shown brain exposure at the level of established CNS-drugs.[19,20] This paradigm, applied to human subjects, might provide important data to further evaluate the effect of osimertinib in patients with brain metastases including those with leptomeningeal metastases.

The aim of the present study was to examine the blood–brain barrier (BBB) penetration, distribution and brain exposure of ^{11}C-osimertinib in healthy human subjects who have an intact BBB. For this purpose, ^{11}C-osimertinib was administered intravenously in microdoses (1.1–1.4 μg) to eight male subjects. The exposure and regional distribution of ^{11}C-osimertinib in brain was measured with a high-resolution PET system and quantified using standard pharmacokinetic parameters as well as a kinetic analysis with compartmental modeling.

Methods

Subjects

Eight healthy male subjects (mean age 52 years, range 44–62 years) participated in the study. The subjects were recruited through advertisement in a local newspaper. They were healthy according to medical history, physical examination, ECG, vital signs, routine blood laboratory health screen and urine test for drug abuse. All subjects had normal collateral circulation between radial and ulnar arteries in at least one hand assessed with the Allen's test. No anatomical brain abnormalities were detected by magnetic resonance imaging (MRI). The study was approved by the Ethical Committee of the Stockholm region, by the Radiation Safety Committee of the Karolinska University Hospital, and by the Medical Products Agency in Sweden (Trial registration: Clinical trial EudraCT no. 2016-004160-19). All procedures performed in studies involving human participants were in accordance with the ethical standards of the institutional and/or national research committee and with the 1964 Helsinki declaration and its later amendments or comparable ethical standards. Written informed consent was obtained from all subjects who participated in the study.

Magnetic resonance imaging

MRI scans were performed with a GE DISCOVERY MR750 system (General Electric, USA). The MR protocol included T2-weighted and FLAIR sequences used for clinical evaluation and exclusion of pathology. The third T1-weighted sequence was used for delineation of anatomically defined brain regions of interests (ROIs). The T1-weighted sequence was a 3D FSPGR BRAVO with the following parameters: TR: 8.1 ms, TE: 3.2 ms, FOV: 256 mm, Matrix: 256 × 256, Slice thickness: 1.0 mm, Pixel size: 1 mm × 1 mm, Flip angle: 12, Prep Time: 450 ms, NEX: 1.

PET experimental procedures

Individualized plaster helmets were made for each subject and used with a head fixation system. The subject

was placed recumbent with his head in the PET system. A cannula was inserted into the left or right cubital vein and another cannula into the radial artery on the opposite side. A sterile physiological phosphate buffer (pH 7.4) solution containing ^{11}C-osimertinib was injected as a bolus within 10 s into the antecubital vein. The cannula was then immediately flushed with 10 ml saline.

PET measurements were performed with a high-resolution research tomograph (HRRT) system (Siemens Medical Imaging). List mode data were acquired for 93 min and reconstructed into frames of increasing duration (9×10 s, 2×15 s, 3×20 s, 4×30 s, 4×1 min, 4×3 min, 12×6 min) using the ordinary Poisson-3D-ordered subset expectation maximization algorithm, with 10 iterations and 16 subsets including modelling of the point spread function. The corresponding in-plane resolution with ordinary Poisson-3D-ordered subset expectation maximization point spread function was 1.5 mm in the centre of the field of view and 2.4 mm at 10-cm off-centre directions.[21] Attenuation correction was acquired with a 6-min transmission measurement using a single ^{137}Cs source.

Arterial blood sampling was performed automatically using a blood sampling system (ABSS, Allogg, Sweden) for the first 10 min and manually thereafter. Region-of-interest analysis was done using the automated anatomical labeling template.

Radiolabelling of osimertinib

No-carrier-added ^{11}C–CH_4 was produced using 16.5 MeV protons in the $^{14}N(p,\alpha)^{11}C$ nuclear reaction on a mixture of nitrogen and hydrogen gas (10% hydrogen). ^{11}C–CH_4 was converted to ^{11}C–CH_3I by radical iodination in a gas-phase recirculation system and swept in a stream of helium through a heated glass column containing silver triflate impregnated on graphpac to produce ^{11}C–CH_3OTf. The radiolabeling agent was bubbled through a solution of precursor (AZ13774738, 0.6–1.0 mg) and aqueous sodium hydroxide (0.5 M, 5 µL) in acetone (400 µL) at room temperature. After 3 min, the reaction mixture was diluted with mobile phase and purified by semi-preparative HPLC using a reversed-phase C-18 column (ACE-C18, 5 µm, 7.8×300 mm, Waters) with MeCN/ammonium formate 45:55 (v/v) and sodium ascorbate (0.5 g/L) as eluent at 6 mL/min. The column outlet was connected with an UV absorbance detector ($\lambda = 254$ nm) in series with a detector for radioactivity. The purified product was diluted in sterile water (50 mL) containing sodium ascorbate (1 mg/mL) and was subsequently loaded on to an Oasis® HLB 1cc cartridge (Waters) previously conditioned with ethanol (10 mL) and sterile water containing sodium ascorbate (10 mL, 1 mg/mL). After trapping the product, the cartridge was rinsed with sterile water containing sodium ascorbate (8 mL, 1 mg/mL) and ^{11}C-osimertinib was then eluted with 30% ethanol in propylene glycol (3 mL) into 12 ml phosphate-buffered saline (12 mL; pH 7.4) and sodium ascorbate (100 mg). The solution was filtered through a Millex-GV filter unit (0.22 µm) (Millipore, Billerica, MA, USA).

The radiochemical purity was >99%. The mean and standard deviation of the administered mass of ^{11}C-osimertinib was 1.26 ± 0.12 µg (range 1.1 to 1.4 µg). The mean administered radioactivity was 347 ± 51 MBq (range 285 to 435 MBq) and the mean molar activity at time of injection was 141 ± 23 GBq/µmol (range 127 to 182 GBq/µmol).

Radiometabolite analysis

The unchanged fraction ^{11}C-osimertinib and its radioactive metabolites in human plasma were measured using a protein precipitation sample preparation technique in combination with a reversed-phase radio-HPLC method. The blood samples (2 mL) were taken 2, 6, 10, 20 and 30 min after injection of ^{11}C-osimertinib and plasma (0.7 mL) was separated from blood by centrifuging at 6000*g* for 2 min. The obtained plasma was mixed with 0.98 mL of acetonitrile and centrifuged at 2000*g* for 4 min and the supernatant was diluted with 2 mL water and injected into an on-line radio-HPLC system to determine the fraction. The amount of radioactivity in blood, in plasma and left in precipitate was measured separately with a NaI(Tl) well counter (PerkinElmer 2480 Wizard2™, Waltham, MA, USA).

An Agilent 1200 series HPLC instrument with a manual injection valve (7725i, Rheodyne), 5.0 ml loop and a radiation detector (Oyokoken, S-2493Z) housed in a shield of 50 mm thick lead was used for metabolite measurements (the accumulation time of radiation detector was 10 s). Data collection and control of the LC system were performed using chromatographic software (ChemStation Rev. B.04.03; Agilent). Chromatographic separation was performed with an ACE 5 C18-HL column, (250 mm × 10 mm I.D) by gradient elution. Acetonitrile (A) and 10 mM ammonium format (B) were used as the mobile phase at 5.0 mL/min, according to the following program: 0−3.0 min, (A/B) 60:40 → 80:20 v/v; 3.0−5.0 min, (A/B) 80:20 v/v; 5.1−6.0 min, (A/B) 90:10 v/v. The area of each obtained peak in the radiochromatogram was expressed as a percentage of the sum of the areas of all detected radioactive peaks (with decay correction).

Calculations

Several descriptive pharmacokinetic parameters were calculated. These include $C_{max\ (brain)}$, $T_{max\ (brain)}$ and

$AUC_{0–90\,min,\ brain/blood\ ratio}$. In addition, the standard uptake value (SUV = [kBq • cm^{-3}/(MBq injected/body weight]) and the percentage of the injected dose (ID%) in brain at T_{max} were calculated.

Moreover, a quantitative analysis of ^{11}C-osimertinib brain exposure was performed using two-tissue (2T) and one-tissue (1T) compartment models (CM) for reversible radioligand binding, as well as using the 2TCM for irreversible radioligand binding, i.e. the rate constant k_4 was set to zero (Supplementary Figure S1 and Table S1).[22] For that purpose, the arterial plasma curve was corrected for radioactive metabolites and used as input function. Correction for radioactive metabolites was performed using a population-based approach. The individual data of the fraction of parent radioligand in the plasma were fitted in a hierarchical Bayesian framework with individual and population level parameters, with weakly informative priors, to ensure consistency across individual fitted and extrapolated curves.[23] The software used for fitting was CmdStan.[24,25] In this framework, the parent fraction data were described by an empirical model curve consisting of a linear mixture of the Hill and Richards equations.[26] Blood volume correction was performed assuming a blood volume fraction of 5%. The primary outcome measure of the compartment analysis was the total distribution volume (V_T), which is the ratio at steady state between the concentration of the radioligand in brain and the concentration of the radioligand in plasma. The compartment analyses were performed using PMOD v 3.2. The Akaike information criterion[27] and F statistics were used to identify the statistically preferred model configuration.

Results

All eight subjects participated in the study according to the protocol. There were no adverse or clinically detectable pharmacologic effects in any of the eight subjects. One subject experienced an episode of vaso-vagal reaction after placement and removal of the arterial cannula. No significant changes in vital signs were otherwise observed. For technical reasons, part of the list mode PET data was missing in one subject. This subject was excluded from the kinetic analysis.

After i.v. administration of ^{11}C-osimertinib, radioactivity appeared rapidly in brain (Figure 1). Injected radioactivity in blood reached its peak within 1 min after radioligand injection, followed by a rapid decrease during the initial 5 min of measurement. The rate of elimination of radioactivity from plasma was slow at later time (25–90 min) after injection (Figure 2(a)).

The mean T_{max} was 13 min (range 5–30 min), a time at which 2.2 ± 0.2% of injected radioactivity was in brain. The C_{max} was 1.5 ± 0.2 SUV (range 1–1.8) (Figure 2(b)), and the $AUC_{0–90\,min\ brain/blood\ ratio}$ was 3.8 ± 0.3 (range 3.3–4.1).

Brain radioactivity was generally higher in grey matter than in white matter (Figures 1 and 2(c)). Among grey matter regions, ^{11}C-osimertinib binding was highest in putamen followed by thalamus, frontal cortex, temporal cortex, caudate, and cerebellum (Figure 2(c)).

The HPLC analysis of unchanged ^{11}C-osimertinib and radioactive metabolites was only performed up to 30 min due to the low radioactivity concentration in the plasma samples. The fraction of unchanged ^{11}C-osimertinib in plasma was 73 ± 8% at 30 min.

The metabolite-corrected arterial input function generated with the population-based approach (Supplementary Figure S2) was used for the subsequent compartment analyses. Based on AIC and F statistics, the 2TCM was statistically preferred over the 1TCM for whole brain and gray matter regions, whereas the 1TCM was sufficient to describe curves for white matter (Figure 2(d); Supplementary Table S2). The regional influx rate constant, K_1, the rate constants k_2, k_3, and k_4, and V_T values are presented in Table 1. Mean V_T of the whole brain was 14 mL × cm^{-3} (range 11–18). Among gray matter regions, V_T was highest for the putamen (17 mL × cm^{-3}, range 13–24) and lowest for cerebellum (13 mL × cm^{-3}, range 10–16). Mean V_T of white matter was 7 mL × $cm^{\times 3}$ (range 5–12).

For all subjects and regions examined, estimates of k_4 were consistently above zero (Table 1). The standard

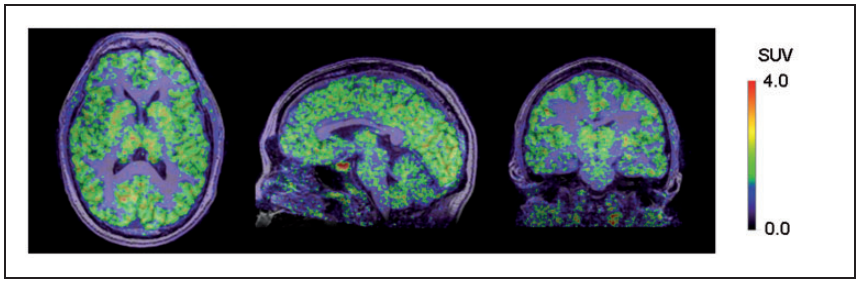

Figure 1. Representative PET images for ^{11}C-osimertinib overlaid on an MRI in a human subject.

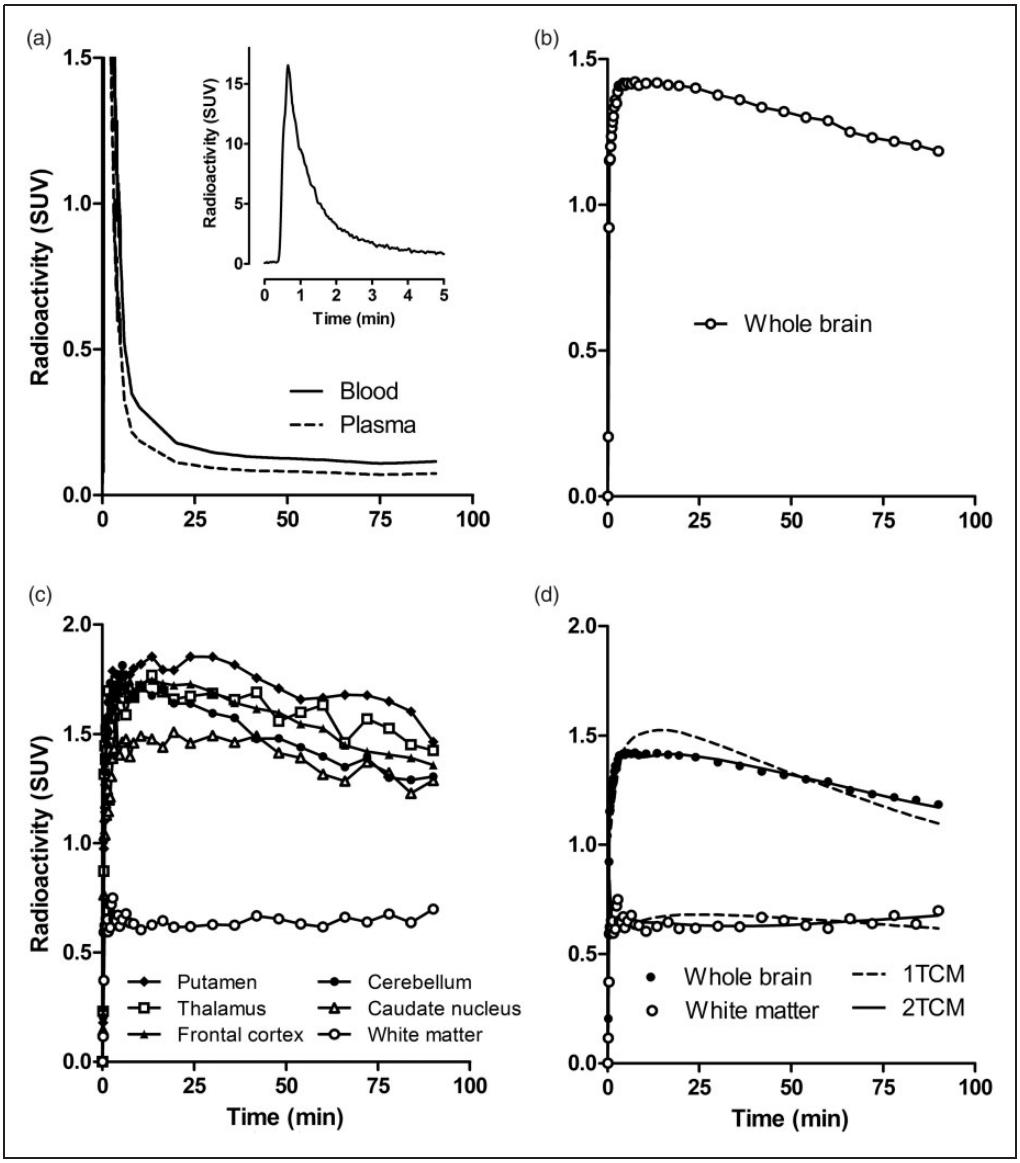

Figure 2. Time activity curves for ^{11}C-osimertinib in a human subject (subject 4). (a) Total radioactivity concentration in blood and radioactivity concentration for parent radioligand in plasma. Inset shows blood radioactivity concentration during the initial five minutes after injection. Whole brain (b) and regional radioactivity (c). Experimental values for the whole brain and white matter with corresponding fitted curves as obtained by the 1TCM and 2TCM (d).

2TCM was statistically preferred over a 2TCM with irreversible binding to the second compartment, i.e. k_4 set to zero (Supplementary Table S3).

Discussion

This PET-study was designed to measure the brain exposure of ^{11}C-labelled osimertinib administered intravenously at microdoses in healthy subjects who have an intact BBB. The primary objective was to obtain quantitative pharmacokinetic parameters that provide a measure of BBB penetration and brain exposure. In addition, kinetic analysis with compartmental modeling was performed using a metabolite corrected arterial input function. Here, the quantitative outcome measure was the total distribution volume (V_T) which indicates the ratio between the concentration of the radioligand in brain and plasma at steady state.

Pharmacokinetic analysis

The pharmacokinetic parameters obtained indicate that ^{11}C-osimertinib crosses the blood–brain barrier rapidly, with a mean T_{max} of 13 min, at which time approximately 2% of the injected radioactivity had entered the brain and was approximately four times higher

Table 1. Rate constants (K_1, k_2, k_3, k_4) and total volume of distribution (V_T) for ^{11}C-osimertinib obtained using a two-tissue compartment model.

Brain region	K_1 (mL·cm^{-3}·min^{-1})	k_2 (min^{-1})	k_3 (min^{-1})	k_4 (min^{-1})	V_T (mL·cm^{-3})
Caudate nucleus	0.16 (0.11–0.18)	0.03 (0.01–0.05)	0.13 (0.02–0.21)	0.34 (0.05–1.99)	15 (11–21)
Cerebellum	0.22 (0.14–0.24)	0.13 (0.09–0.18)	0.28 (0.15–0.40)	0.04 (0.03–0.04)	13 (10–16)
Frontal cortex	0.21 (0.14–0.23)	0.09 (0.04–0.28)	0.27 (0.12–0.58)	0.08 (0.03–0.24)	15 (12–22)
Insular cortex	0.21 (0.13–0.30)	0.33 (0.06–1.62)	0.49 (0.12–1.62)	0.03 (0.02–0.05)	16 (12–23)
Limbic cortices	0.18 (0.12–0.21)	0.11 (0.05–0.20)	0.29 (0.16–0.55)	0.04 (0.03–0.06)	14 (10–19)
Occipital cortex	0.30 (0.21–0.37)	0.73 (0.10–1.78)	0.96 (0.23–1.84)	0.03 (0.02–0.05)	16 (13–20)
Parietal cortex	0.23 (0.18–0.27)	0.18 (0.04–0.56)	0.41 (0.11–0.87)	0.05 (0.03–0.08)	16 (13–22)
Putamen	0.21 (0.14–0.24)	0.06 (0.02–0.16)	0.21 (0.06–0.59)	0.07 (0.04–0.21)	17 (13–24)
Temporal cortex	0.20 (0.13–0.24)	0.14 (0.06–0.41)	0.37 (0.15–0.97)	0.04 (0.03–0.08)	16 (12–22)
Thalamus	0.23 (0.14–0.34)	0.38 (0.03–1.91)	0.51 (0.14–2.07)	0.04 (0.02–0.06)	16 (13–23)
Whole brain	0.17 (0.12-0.19)	0.08 (0.04-0.14)	0.19 (0.11-0.29)	0.04 (0.03-0.07)	14 (11-18)

Note: Data are presented as mean and range for seven subjects.

than the blood exposure. The T_{max}, C_{max} and $AUC_{0–90\,min\ brain/blood\ ratio}$ values were in the same range as those previously reported for reference CNS drugs using the same methodology in non-human primates.[20] These pharmacokinetic observations and the similarities to established CNS-drugs support the view that osimertinib has excellent brain exposure and hence potential for the treatment of brain metastases in EGFRm NSCLC patients. The BBB penetration can of course be also dependent on the lipophilicity and protein binding of a drug. Osimertinib is a lipophilic compound (calculated LogP = 4.8) with a plasma protein binding of 94.7% measured in vitro.[28] Previous studies have shown that the recovery of osimertinib in human plasma and human serum albumin is particularly low even using the equilibrium dialysis method.[29] For this reason, the plasma protein binding was not measured in this study.

To examine the metabolism of ^{11}C-osimertinib in vivo, HPLC analysis was performed on arterial plasma samples. The fraction of unchanged ^{11}C-osimertinib in plasma was measured only for the first 30 min after injection, due to low plasma radioactivity, most likely related to the large volume of distribution of osimertinib.[30] The unchanged radioligand represented approximately 70% of the total radioactivity in plasma at 30 min, suggesting that ^{11}C-osimertinib is rather stable in plasma. In support of these observations, previous studies with ^{14}C-labelled osimertinib performed in healthy volunteers at steady state after oral administration have indicated that no more than 10% of the total radioactivity is related to metabolites of osimertinib and that the T_{max} of the two major metabolites was 33 and 42 h, respectively, after IV administration of osimertinib.[30] Therefore, after IV administration of ^{11}C-osimertinib, because of the slow kinetics of the two major metabolites, there is a low likelihood of observing relevant fractions of radiometabolites in plasma and brain within the short time frame of a PET measurement.

Brain distribution and quantification of ^{11}C-osimertinib binding

The distribution of ^{11}C-osimertinib in the brain of healthy volunteers showed that the radioactivity is distributed across all regions of the brain (Figures 1 and 2(c)). The kinetic analysis was performed using compartmental models for reversible and irreversible radioligand binding.

In all grey matter regions, the 2TCM with four rate constants (reversible model) was the statistically preferred model, indicating that the kinetics of ^{11}C-osimertinib in the healthy brain can be described by two compartments with passive diffusion of the radioligand between compartments and without irreversible binding or metabolic trapping. Osimertinib has been shown in experimental animals to bind to the EGFR sensitizing mutation and the resistant T790M mutation in an irreversible manner.[29] The reversible nature of the binding kinetics of ^{11}C-osimertinib observed in the present study within the time frame of the PET measurements is reasonably explained by the lack of the EGFRm receptor in the brain of healthy volunteers.

The K_1 values obtained by 2TCM were similar to those reported for established neuroreceptor radioligands such as ^{11}C-raclopride[31] and in line with the early T_{max} of osimertinib. The lowest K_1 value was obtained for the caudate ($0.11\,mL \cdot cm^{-3} \cdot min^{-1}$) and the highest for the occipital cortex ($0.37\,mL \cdot cm^{-3} \cdot min^{-1}$). In the remaining regions, K_1 ranged between 0.12 and $0.30\,mL \cdot cm^{-3} \cdot min^{-1}$. Assuming a cerebral blood flow of $50\,mL \cdot 100\,g \cdot min^{-1}$ and a density of brain tissue of $1\,g \cdot cm^{-3}$, the average

first pass extraction of ^{11}C-osimertinib for the whole brain would be approximately 30%. This estimate of first pass extraction is again similar to the one reported for ^{11}C-raclopride[31] and consistent with the presence of an intact BBB.

A population-based approach was used to obtain a metabolite-corrected arterial input function for the kinetic analysis. The whole brain V_T was $14\,mL \cdot cm^{-3}$, indicating a high partition coefficient between brain and plasma, for instance in comparison with well-established radioligands such as ^{11}C-raclopride (V_T $\sim$0.3–$2\,mL \cdot cm^{-3}$ depending on the brain region)[32] or ^{11}C-flumazenil (V_T $\sim$3–$6\,mL \cdot cm^{-3}$ depending on the brain region).[33] Regional V_T values ranged between 13 and $17\,mL \cdot cm^{-3}$, indicating that ^{11}C-osimertinib is rather homogeneously distributed in gray matter.

The reversible type of kinetic behavior observed for ^{11}C-osimertinib is a common observation for radioligands that bind specifically to brain receptors, transporters or enzymes. In such setting, the two compartments are thought to represent non-displaceable and specific binding. On the other hand, in white matter, the preferred quantification model was the 1TCM. This observation does not support the existence of a specific binding compartment in white matter. Taken together, it cannot be excluded that a fraction of ^{11}C-osimertinib binding in gray matter may represent specific binding to non-mutated or wild-type EGFR.

Specific binding of osimertinib

Biochemical characterization of the drug has shown that osimertinib displays nearly 200-fold greater affinity for the EGFR with T790M/L858R mutation (apparent IC_{50} of 1 nM) than for the EGFR wild-type (apparent IC_{50} 184 nM).[12] EGFR is widely expressed in the normal brain in neurons (cortical pyramidal cells and Purkinje cells of cerebellum) and ependymal cells.[34,35] The broad distribution of ^{11}C-osimertinib in the human brain is therefore consistent with the wide expression of the EGFR. However, considering the low apparent affinity of osimertinib for the wild-type EGFR, it cannot be excluded that the uptake observed in the healthy brain could be non-specific.

Future directions

This study has examined the pharmacokinetic properties of ^{11}C-osimertinib in healthy subjects. Considering the affinity of osimertinib towards the T790M/L858R EGFRm+, an ongoing study of the kinetic behavior of ^{11}C-osimertinib in patients with metastatic NSCLC and brain metastases (NCT03463525) will provide additional information on the pharmacodynamic potential of osimertinib for the treatment of brain metastases.

Conclusions

This study showed that ^{11}C-osimertinib enters the brain rapidly with an exposure of 2% of injected dose at T_{max} (range from 1.7 to 2.4%). This brain exposure is similar to that for well-established CNS drugs. The pharmacokinetic observations of the present study, the similarity with established CNS-drugs, along with recent evidence of CNS efficacy, support the view that osimertinib has potential for the treatment of EGFRm-positive NSCLC patients with brain metastases. The approach presented in this study further illustrates the role of molecular imaging in facilitating the development of novel drugs for the treatment of malignancies.

Funding

The author(s) disclosed receipt of the following financial support for the research, authorship, and/or publication of this article: This study was funded by AstraZeneca, project number: ESR-17-12920.

Acknowledgments

The authors thank the staff of the PET-Centre at Karolinska Institutet for their technical support.

Declaration of conflicting interests

The author(s) declared the following potential conflicts of interest with respect to the research, authorship, and/or publication of this article: Andrea Varrone has received research grants from the Swedish Science Council, the Michael J Fox Foundation, Vinnova, Åhlens Foundation, a private donation and the Swedish Brain Foundation.
Aurelija Jucaite, Zsolt Cselenyi, Peter Johnström, Magnus Schou, Andrew P Brown, Karthick Vishwanathan and Lars Farde are employed and own stocks of AstraZeneca. Katarina Varnäs has received a consulting fee from AstraZeneca.
Christer Halldin, Ana Vazquez-Romero, and Mohammad Mahdi Moein declare no conflict of interest.

Authors' contributions

The specific contribution of each author is described as follows:
Andrea Varrone: Contributing to conception and design, acquisition of data, interpretation of data; drafting and revising the manuscript, as well as enhancing its intellectual content; approving the final content of the manuscript.
Katarina Varnäs: Contributing to analysis and interpretation of data; drafting and revising the manuscript, as well as enhancing its intellectual content; approving the final content of the manuscript.
Aurelija Jucaite: Contributing to conception and design, interpretation of data; drafting and revising the manuscript, as well as enhancing its intellectual content; approving the final content of the manuscript.
Zsolt Cselényi: Contributing to conception and design, analysis and interpretation of data; revising the manuscript; approving the final content of the manuscript.
Peter Johnström: Contributing to conception and design, acquisition of data, interpretation of data; drafting and

revising the manuscript, as well as enhancing its intellectual content; approving the final content of the manuscript.
Magnus Schou: Contributing to conception and design, acquisition of data, interpretation of data; revising the manuscript; approving the final content of the manuscript.
Ana Vazquez-Romero: Contributing to acquisition of data; drafting the manuscript; approving the final content of the manuscript.
Mohammad Mahdi Moein: Contributing to acquisition, analysis and interpretation of data; drafting the manuscript; approving the final content of the manuscript.
Christer Halldin: Contributing to interpretation of data; revising the manuscript and approving the final content of the manuscript.
Andrew P Brown: Contributing to conception and design, interpretation of data; revising the manuscript, as well as enhancing its intellectual content; approving the final content of the manuscript.
Karthick Vishwanathan: Contributing to conception and design, interpretation of data; revising the manuscript, as well as enhancing its intellectual content; approving the final content of the manuscript.
Lars Farde: Contributing to conception and design, interpretation of data; revising the manuscript, as well as enhancing its intellectual content; approving the final content of the manuscript.

Supplemental Material

Supplemental material for this article is available online.

References

1. Bonomi PD. Implications of key trials in advanced non-small cell lung cancer. *Cancer* 2010; 116: 1155–1164.
2. Heydt C, Michels S, Thress KS, et al. Novel approaches against epidermal growth factor receptor tyrosine kinase inhibitor resistance. *Oncotarget* 2018; 9: 15418–15434.
3. Ahluwalia MS, Becker K and Levy BP. Epidermal growth factor receptor tyrosine kinase inhibitors for central nervous system metastases from non-small cell lung cancer. *Oncologist* 2018; 23: 1199–1209.
4. Vansteenkiste J, Reungwetwattana T, Nakagawa K, et al. CNS response to osimertinib vs standard of care (SoC) EGFR-TKI as first-line therapy in patients (pts) with EGFR-TKI sensitising mutation (EGFRm)-positive advanced non-small cell lung cancer (NSCLC): data from the FLAURA study. *Ann Oncol* 2017; 28: x189.
5. Mujoomdar A, Austin JH, Malhotra R, et al. Clinical predictors of metastatic disease to the brain from non-small cell lung carcinoma: primary tumor size, cell type, and lymph node metastases. *Radiology* 2007; 242: 882–888.
6. Heon S, Yeap BY, Britt GJ, et al. Development of central nervous system metastases in patients with advanced non-small cell lung cancer and somatic EGFR mutations treated with gefitinib or erlotinib. *Clin Cancer Res* 2010; 16: 5873–5882.
7. Arrieta O, Villarreal-Garza C, Zamora J, et al. Long-term survival in patients with non-small cell lung cancer and synchronous brain metastasis treated with whole-brain radiotherapy and thoracic chemoradiation. *Radiat Oncol* 2011; 6: 166.
8. Owen S and Souhami L. The management of brain metastases in non-small cell lung cancer. *Front Oncol* 2014; 4: 248.
9. Rangachari D, Yamaguchi N, VanderLaan PA, et al. Brain metastases in patients with EGFR-mutated or ALK-rearranged non-small-cell lung cancers. *Lung Cancer* 2015; 88: 108–111.
10. Pao W, Miller VA, Politi KA, et al. Acquired resistance of lung adenocarcinomas to gefitinib or erlotinib is associated with a second mutation in the EGFR kinase domain. *PLoS Med* 2005; 2: e73.
11. Finlay MR, Anderton M, Ashton S, et al. Discovery of a potent and selective EGFR inhibitor (AZD9291) of both sensitizing and T790M resistance mutations that spares the wild type form of the receptor. *J Med Chem* 2014; 57: 8249–8267.
12. Cross DA, Ashton SE, Ghiorghiu S, et al. AZD9291, an irreversible EGFR TKI, overcomes T790M-mediated resistance to EGFR inhibitors in lung cancer. *Cancer Discov* 2014; 4: 1046–1061.
13. Koba T, Kijima T, Takimoto T, et al. Rapid intracranial response to osimertinib, without radiotherapy, in non-small cell lung cancer patients harboring the EGFR T790M mutation: two case reports. *Medicine* 2017; 96: e6087.
14. Soria JC, Ohe Y, Vansteenkiste J, et al. Osimertinib in untreated EGFR-mutated advanced non-small-cell lung cancer. *N Engl J Med* 2018; 378: 113–125.
15. Reichegger H, Jochum W, Forbs D, et al. Rapid intracranial response to osimertinib in a patient with epidermal growth factor receptor T790M-positive adenocarcinoma of the lung. *Oncol Res Treat* 2016; 39: 461–463.
16. Chalmers A, Jensen L and Akerley W. Durable response to osimertinib in EGFR mutated T790M wildtype non-small cell lung cancer with leptomeningeal metastases: a case report. *Lung Cancer* 2017; 114: 68–69.
17. Wu YL, Ahn MJ, Garassino MC, et al. CNS efficacy of osimertinib in patients with T790M-positive advanced non-small-cell lung cancer: data from a randomized phase III trial (AURA3). *J Clin Oncol* 2018; 36: 2702–2709.
18. Reungwetwattana T, Nakagawa K, Cho BC, et al. CNS response to osimertinib versus standard epidermal growth factor receptor tyrosine kinase inhibitors in patients with untreated EGFR-mutated advanced non-small-cell lung cancer. *J Clin Oncol* 2018; 36: 3290–3297.
19. Ballard P, Yates JW, Yang Z, et al. Preclinical comparison of osimertinib with other EGFR-TKIs in EGFR-mutant NSCLC brain metastases models, and early evidence of clinical brain metastases activity. *Clin Cancer Res* 2016; 22: 5130–5140.
20. Schou M, Varnäs K, Lundquist S, et al. Large variation in brain exposure of reference CNS drugs: a PET study in nonhuman primates. *Int J Neuropsychopharmacol* 2015; 18: pyv036.
21. Varrone A, Sjöholm N, Eriksson L, et al. Advancement in PET quantification using 3D-OP-OSEM point spread function reconstruction with the HRRT. *Eur J Nucl Med Mol Imaging* 2009; 36: 1639–1650.

22. Varnäs K, Varrone A and Farde L. Modeling of PET data in CNS drug discovery and development. *J Pharmacokinet Pharmacodyn* 2013; 40: 267–279.
23. Gelman A, Carlin JB, Stern HS, et al. Hierarchical models. Bayesian data analysis. Boca Raton, FL, USA: CRC Press Taylor & Francis Group, 2013, pp.101–138.
24. Carpenter B, Gelman A, Hoffman MD, et al. Stan: a probabilistic programming language. *J Stat Software* 2017; 76: 1–29.
25. Stan Development Team. *CmdStan: the command-line interface to Stan*, 2015. Available at: https://mc-stan.org/users/interfaces/cmdstan.
26. Bindslev N. *Hill in hell. Drug-acceptor interactions modeling theoretical tools to test and evaluate experimental equilibrium effects*. Routledge: Taylor and Francis Group, 2008, pp.257–282.
27. Akaike H. A new look at the statistical model identification. *IEEE Transac Automatic Control* 1974; 19: 716–723.
28. European Medicine Agency. Tagrisso – product information, www.ema.europa.eu/en/medicines/human/EPAR/tagrisso (2016, accessed 17 February 2016).
29. Dickinson PA, Cantarini MV, Collier J, et al. Metabolic disposition of osimertinib in rats, dogs, and humans: insights into a drug designed to bind covalently to a cysteine residue of epidermal growth factor receptor. *Drug Metab Dispos* 2016; 44: 1201–1212.
30. Vishwanathan K, So K, Thomas K, et al. Absolute bioavailability of osimertinib in healthy adults. *Clin Pharmacol Drug Dev* 2019; 8: 198–207.
31. Farde L, Eriksson L, Blomquist G, et al. Kinetic analysis of central [^{11}C]raclopride binding to D2-dopamine receptors studied by PET – a comparison to the equilibrium analysis. *J Cereb Blood Flow Metab* 1989; 9: 696–708.
32. Schain M, Fazio P, Mrzljak L, et al. Revisiting the Logan plot to account for non-negligible blood volume in brain tissue. *EJNMMI Res* 2017; 7: 66.
33. Odano I, Halldin C, Karlsson P, et al. [^{18}F]flumazenil binding to central benzodiazepine receptor studies by PET – quantitative analysis and comparisons with [^{11}C]flumazenil. *Neuroimage* 2009; 45: 891–902.
34. Birecree E, King LE Jr. and Nanney LB. Epidermal growth factor and its receptor in the developing human nervous system. *Brain Res Dev Brain Res* 1991; 60: 145–154.
35. Werner MH, Nanney LB, Stoscheck CM, et al. Localization of immunoreactive epidermal growth factor receptors in human nervous system. *J Histochem Cytochem* 1988; 36: 81–86.